

Learning Post-Newtonian Corrections from Numerical Relativity

Jooheon Yoo ^{1,*} Michael Boyle ¹ and Nils Deppe ¹

¹*Cornell Center for Astrophysics and Planetary Science, Cornell University, Ithaca, New York 14853, USA*

(Dated: December 9, 2025)

Accurate modeling of gravitational waveforms from compact binary coalescences remains central to gravitational-wave (GW) astronomy. Post-Newtonian (PN) approximations capture the early inspiral dynamics analytically but break down near merger, while numerical relativity (NR) provides the accurate yet computationally expensive waveforms over limited parameter ranges. We develop a physics-informed neural network (PINN) framework that learns corrections mapping PN dynamics and waveforms to their NR counterparts. As a demonstration of the approach, we use the TaylorT4 PN model as the baseline, and train the network on a remarkably small dataset of only eight hybridized NR surrogate waveforms (NRHybSur3dq8) to learn higher-order corrections to the orbital dynamics and waveform modes for nonspinning noneccentric systems. Physically motivated loss terms enforce known limits and symmetries, such as vanishing corrections in the Newtonian limit and suppression of odd- m modes in equal-mass systems, promoting consistent and reliable extrapolation beyond the training region. We simultaneously incorporate corrections that account for the different meaning of mass parameters in PN and NR descriptions. The learned corrections significantly reduce the phase and amplitude error through the inspiral up to about $200M$ before the merger. This approach provides a differentiable and computationally efficient bridge between PN and NR, offering a path toward waveform models that generalize more robustly beyond existing NR datasets.

I. INTRODUCTION

Since the landmark discovery of gravitational waves (GWs) from binary black holes (BBHs) in 2015 [1], detections have become increasingly frequent as the sensitivity of ground-based interferometers continues to improve. Recent publication of the loudest observed event [2] highlights the remarkable progress achieved over the past decade. With next-generation detectors on the horizon [3–5], both the detection rate and sensitivity are expected to increase further. Thus, the demand for high fidelity GW templates has become more important than ever.

Numerical relativity (NR) is the only *ab initio* method for solving Einstein’s equations for the mergers of two compact objects and has played a fundamental role in GW theory and GW astronomy [6–10]. Despite many efforts to make these simulations more computationally efficient, they remain prohibitively expensive for direct applications such as source parameter estimation. To address this bottleneck, several waveform models have been developed that provide a faster alternative to evolving an entire NR simulation to generate a GW template.

Effective-one-body (EOB) [11–18] and phenomenological models [19–35] incorporate some known physics, but still require “calibration” to NR waveforms, including careful selection of the parameters to be calibrated, with limited ability to capture physics beyond the currently known analytical behavior. NR surrogate models [36–40] are a more recent addition to the family of BBH waveform models and take a data-driven approach by training directly on the waveform outputs from NR simulations. Consequently, these surrogates reproduce NR waveforms

more faithfully than other semi-analytical models; however, they are limited to regions of parameter space where NR simulations exist. In addition, as NR simulations typically cover only the final ~ 20 orbits before merger, NR-only surrogate models cannot span the full LIGO frequency band. This limitation will become increasingly problematic since both future space-based and ground-based detectors promise sensitivity at even lower frequencies. To address this, hybrid surrogate models have been developed in which hybrid waveforms combining PN-based early inspiral and NR merger-ringdown data are used for training.

In this sense, all three classes of models—surrogate, phenomenological, and EOB—are hybrid models, incorporating some analytical information, and some numerical information. However, discrepancies between lead to imperfect stitching, introducing hybridization errors that can compromise the accuracy of the resulting models [41]. Even the parameters used in the PN and NR descriptions differ; Ref. [42] found that the mass parameters in the two formalisms can differ even at 1PN order, to say nothing of differences in spins and eccentricities. These discrepancies lead to systematic errors when not taken into account in comparing analytic and numerical waveforms. Essentially, the part of the model comprised of analytical information and the part comprised of numerical information describe physically different systems.

As pointed out in recent work [41], there is a trade-off in selecting the hybridization windows. Choosing an earlier window increases errors due to nonzero residual eccentricity in NR simulations, whereas a later window amplifies discrepancies arising from PN’s inaccuracy near merger. This naturally raises the question: can we introduce data-driven higher-order corrections to PN approximations so that they more closely match NR waveforms in the late inspiral regime?

* jy884@cornell.edu

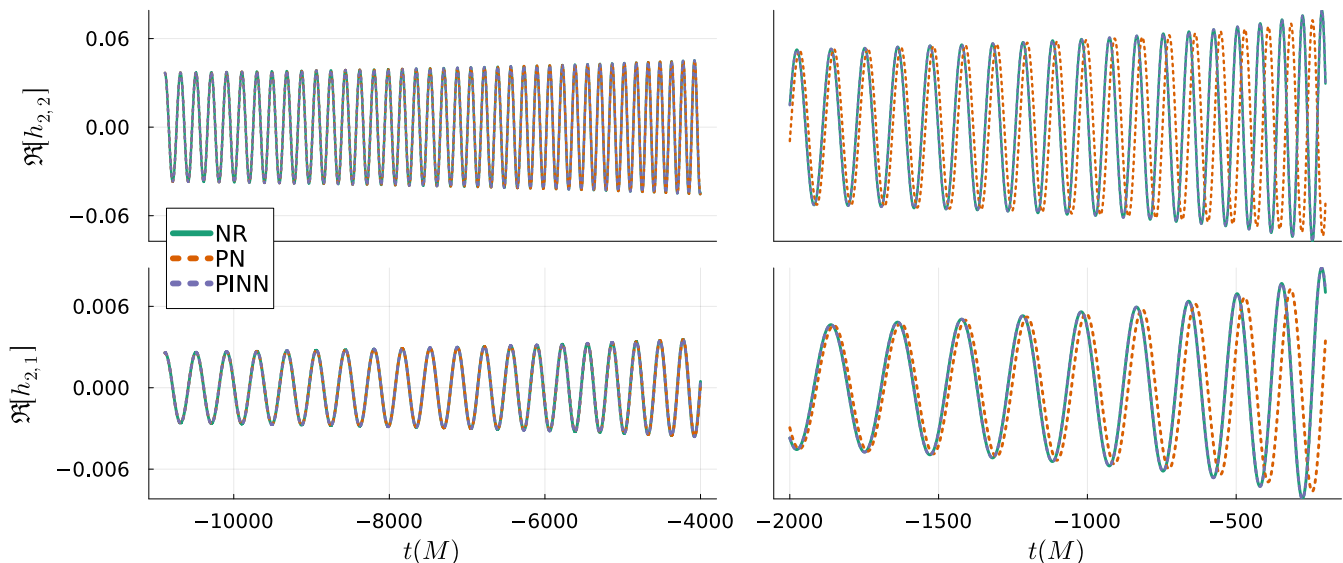


FIG. 1. Real parts of $h_{2,2}$ and $h_{2,1}$ for the highest mass ratio validation case of $q = 7.93$ for the final NN model for PN to NR correction. The waveform mismatch is reduced from 2×10^{-1} to 1×10^{-6} . All waveforms are phase-aligned at start. Although the PN waveform agrees well with NR at early inspiral parts, it deviates significantly near merger where both phase and amplitude discrepancies emerge. The NN corrections significantly reduce these discrepancies, allowing the PN waveforms to remain consistent with NR counterparts in the late inspiral regime.

In recent years, neural networks have emerged as versatile tools in computational physics, capable of modeling complex nonlinear dependencies. In the field of GW astronomy, they have been applied to a wide range of problems including waveform modeling, parameter estimation, and detection classification [43–45]. One application is the use of physics-informed neural networks (PINNs), which incorporate physical results or principles into the neural network design or training process [46–53].¹ In particular, Keith *et al.* [54] explored the use of neural networks to learn relativistic orbital corrections to Newtonian dynamics directly from GW data. Building upon this idea, we investigate whether neural networks can learn higher order corrections to PN approximations to bridge the gap between PN and NR waveforms.

To explore this potential, we develop a neural-network based framework that learns the physics-informed corrections that map PN dynamics and waveforms to their NR counterparts. The network is designed to augment the existing PN formalism by learning residual correction terms that can account for the higher-order missing physics in the standard PN expansion.

By anchoring the model to known PN dynamics, we effectively embed physical information into the learning process, ensuring that the network’s corrections remain consistent with well-understood analytical behavior. In

addition, physics-based loss terms impose constraints on these corrections which regularize the solution and promote physically meaningful extrapolation beyond training region. As a first step forward in this framework, we focus on nonspinning, noneccentric system. In this work, we train the model on a small set of eight hybrid NR surrogate waveforms, demonstrating the framework’s potential for data efficient PN to NR calibration.

The rest of the paper is organized as follows. In Sec. II, we describe results from a toy problem where we learn the 3PN terms using a neural network-augmented 2PN evolution. This serves as a controlled test of our framework and demonstrates the network’s ability to reproduce analytically known higher-order corrections. Section III presents the full framework that extends this approach to learning corrections from the PN model to NR waveforms, including network architecture, data preparation, and implementation details. Its subsections describe the loss functions, examine the framework’s extrapolation behavior beyond the training region, and explore how incorporating a small amount of additional training data can further improve model accuracy. Finally, in Sec. IV, we summarize our findings and discuss potential avenues for extending the framework to a broader region of parameter space.

II. 2PN \rightarrow 3PN EXPERIMENT

The primary objective of this study is to evaluate whether a neural network can effectively learn physics-informed corrections that reduce discrepancies between

¹ Neural ODEs, universal differential equations, and physics-informed neural networks are sometimes distinguished in the literature; here we simply refer to them collectively as PINNs.

PN and NR waveforms near merger.

Before applying the framework to NR data, we first test it on a simpler, analytically controlled problem: learning the corrections required to map the 2PN approximation to the 3PN approximation. This serves as a proof of concept, verifying that the network can recover known higher-order terms when trained on data generated purely from PN theory. Since both 2PN and 3PN expression are analytically known, this experiment provides a clean test bed for assessing the network’s capacity to represent higher-order corrections.

The difference between the 2PN and 3PN waveforms arises from two main sources: (i) missing higher-order terms in the orbital dynamics, represented by the right-hand side of the evolution equation for the orbital velocity \dot{v} , and (ii) missing higher-order terms in the waveform amplitude and phase. To address both effects simultaneously, we employ a neural-network architecture with multiple outputs: one branch predicting corrections to the orbital dynamics, and another predicting corrections to the dominant waveform modes, $h_{2,2}$ and $h_{2,1}$. The overall design of this 2PN \rightarrow 3PN experiment is illustrated in Fig. 2.

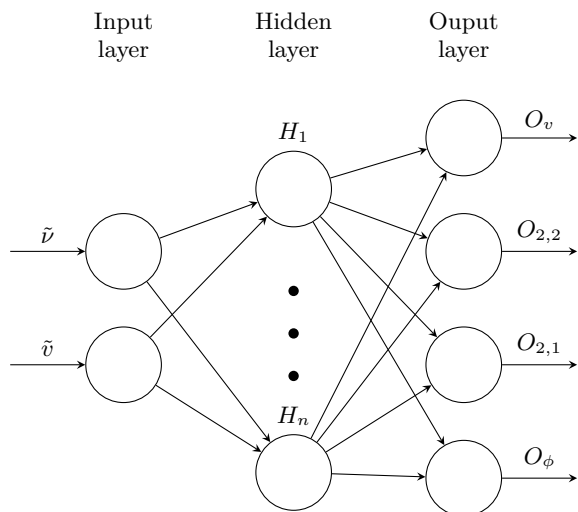


FIG. 2. Neural network architecture for the 2PN \rightarrow 3PN experiment. The two inputs, (ν, v) , are linearly rescaled to the interval $[-1, 1]$ to improve numerical stability during training. Each network output is multiplied by a tunable scaling coefficient before being applied as a correction to either the orbital dynamics or the waveform modes. The final architecture uses a single hidden layer with eight neurons.

To ensure stable training and well-conditioned gradients, both inputs, the symmetric mass ratio ν and the orbital velocity v , are linearly rescaled to the interval $[-1, 1]$ before being passed into the network. The rescaled inputs, denoted by $\tilde{\nu}$ and \tilde{v} are obtained by applying linear transformation such that $\nu \in [0.09, 0.25]$ and $v \in [0.24, 0.36]$ map to the range $[-1, 1]$. These bounds are chosen to be slightly wider than the actual training data range to avoid boundary effects and to maintain consistent behavior near

the edges.

The orbital dynamics are governed by a PN expansion in powers of v , truncated at a given PN order:

$$\dot{v} = c_0(1 + c_1v + c_2v^2 + \dots + c_{2n}v^{2n}), \quad (1)$$

where c_0 represents the leading-order Newtonian contribution, and n represent the PN order. The neural network is trained to learn the missing contribution between the 2PN and 3PN truncations, $O_v(\nu, v)$. The NN correction to the orbital dynamics can be written as

$$\dot{v}_{\text{corr}} = \dot{v}_{2\text{PN}} + c_0 \beta_v O_v(\nu, v) v^5, \quad (2)$$

where β is a tunable scaling coefficient, and $O_v(\nu, v)$ is the neural-network prediction representing the higher-order correction.

In earlier attempts, we allowed the network to output two independent coefficients corresponding to the v^5 and v^6 terms separately. However, we found that these corrections were highly degenerate: the network tended to fit combinations of coefficients that produces nearly identical effects on the orbital evolution. Empirically, we observed that one term is sufficient to model the overall difference between $\dot{v}_{2\text{PN}}$ and $\dot{v}_{3\text{PN}}$.

The PN waveform modes are likewise expanded and truncated in (v/c) , necessitating corrections to both amplitude and phase for each mode. The neural-network-predicted corrections are applied as

$$\begin{aligned} h'_{2,2} &= h_{2,2}(1 + \beta_{2,2}O_{2,2}(\nu, v))e^{2\beta_\phi O_\phi(\nu, v)} \\ h'_{2,1} &= h_{2,1}(1 + \beta_{2,1}O_{2,1}(\nu, v))e^{\beta_\phi O_\phi(\nu, v)} \end{aligned} \quad (3)$$

Each of the neural-network outputs $O_{2,2}$, $O_{2,1}$, and O_ϕ is multiplied by its own scaling coefficient β 's before being applied. These coefficients act as tunable hyperparameters that control the relative strength of each correction during training, ensuring balanced convergence between the amplitude and phase components.

The overall 2PN \rightarrow 3PN procedure can be summarized as:

1. Apply the correction $O_v(\nu, v)$ to the 2PN expression for \dot{v} following Eq. (2).
2. Integrate the resulting ODE to obtain the corrected orbital evolution.
3. Compute the waveform modes $h_{2,2}$ and $h_{2,1}$ from the corrected orbital evolution.
4. Apply the waveform mode correction as described in Eq. (3)

The training data consist of 3PN waveforms sampled on a uniform grid in the symmetric mass ratio ν . Specifically, we generate waveforms for values of $q \in [1, 8]$ uniformly distributed in ν and segment each waveform into uniform Δv intervals within $v \in [0.3, 0.35]$. The network is first trained on these segmented waveforms to accelerate the

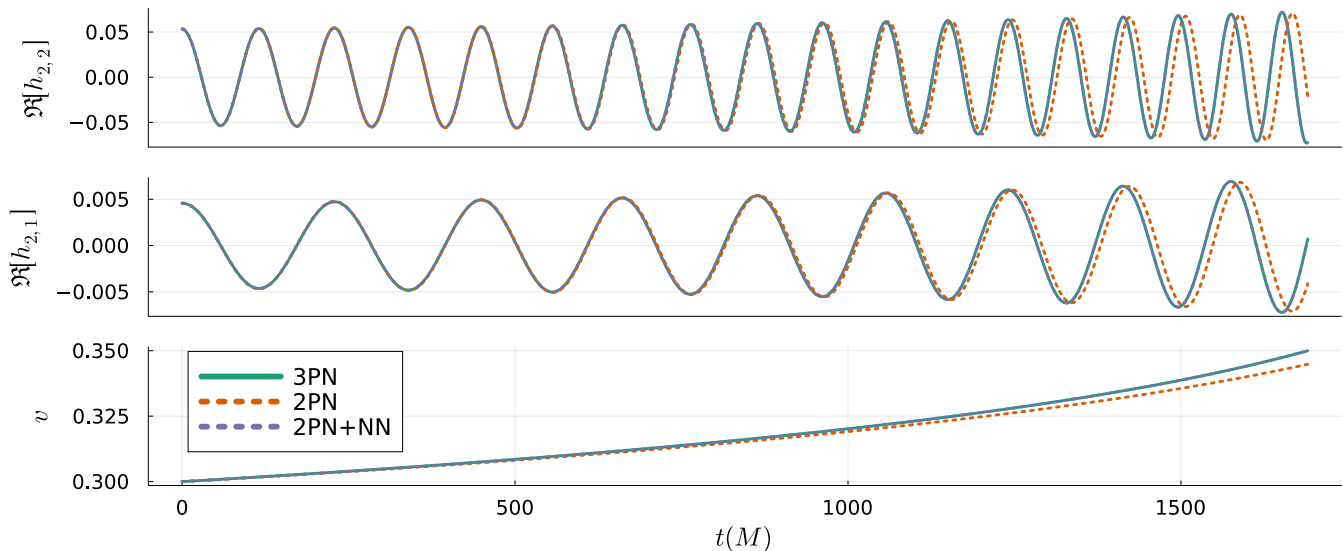


FIG. 3. Real part of the $h_{2,2}$ and $h_{2,1}$ and the orbital velocity v , for the worst validation case ($q = 7.84$). Including the NN corrections reduces the mismatch from 10^{-1} to 4×10^{-8} . All the waveforms are phase-aligned at $t = 0$. The consistent improvement in the corrected orbital velocity shows that the NN captures genuine orbital corrections rather than simply compensating through the waveform modes corrections.

learning of the v -dependence of the corrections, following a strategy conceptually similar to multiple-shooting methods. The network is then refined using full waveforms to ensure global consistency in the corrections across the inspiral.

The network is trained by minimizing the mean waveform mismatch over all training samples. For each sample, we compute the mismatch between the reference 3PN waveform and the neural-network-corrected 2PN waveform obtained through the correction procedure outlined above. The mismatch between two waveforms are computed as

$$\Delta(h_1, h_2) = \frac{1}{2} \frac{\|h_1 - h_2\|^2}{\sqrt{\|h_1\|^2 \|h_2\|^2}}. \quad (4)$$

where $\| \cdot \|$ represents complex inner product defined as:

$$\|h_1, h_2\|^2 = \sum_{t=t_0}^{t_f} h_1^\dagger(t) h_2(t). \quad (5)$$

To prevent overfitting, we include a regularization term weighted by a hyperparameter λ_{L_2} in the final loss function,

$$\mathcal{L}_{\text{total}} = \langle \mathcal{L}_{\text{waveform}} \rangle + \lambda_{L_2} \sum_n (\theta_n^{\text{NN}})^2, \quad (6)$$

For this experiment, we used L_2 regularization defined from the squared L_2 norm of the network parameters only including the weights.²

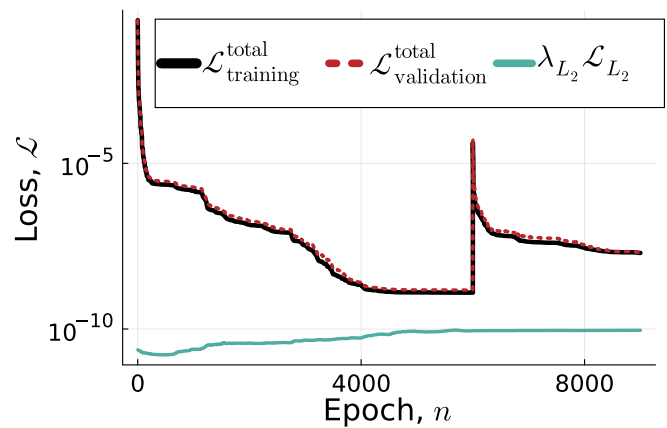


FIG. 4. Training and validation loss history for the 2PN \rightarrow 3PN experiment. The validation losses closely follow the training losses, indicating that the neural network generalizes beyond the training set. The sharp increase in loss near epoch, $n = 6000$, corresponds to the transition from segmented-waveform training to full-waveform training.

We use the quasi-Newton BFGS routine for optimization. We also experimented with adaptive methods such as Adam [55] optimizer, but found that, given the small training data size and relatively small network size the multi-batching advantages of Adam could not be fully

² Because the purpose of regularization is preventing overfitting,

we only want to penalize the weights that affect the sensitivity of the outputs to the inputs and not the biases.

exploited for the given framework.

The network achieves an average waveform mismatch on the order of 10^{-8} between 3PN and NN-corrected 2PN waveforms over the training range of $q \in [1, 8]$. To confirm generalization, 20% of the data are withheld for validation at the start of the training. The training and validation losses converges to the same tolerance as shown in Fig. 4. The sharp increase in loss around epoch³, $n = 6000$, marks the transition from segmented-waveform training to full-waveform training.

Because the loss function is defined solely in terms of waveform mismatch, the orbital and mode corrections can exhibit degeneracy, where different combinations of corrections yield nearly identical waveform errors. For example, the NN could overemphasize waveform mode correction to compensate for an inaccurately learned orbital correction. To verify that this degeneracy did not lead to poor modeling of the orbital dynamics, we perform additional post-training diagnostics. In particular, we compare the corrected v -trajectories with the reference 3PN results in Fig. 3 alongside the real part of the $h_{2,2}$ and $h_{2,1}$, and examine the learned coefficients of the \dot{v} correction in Fig. 5.

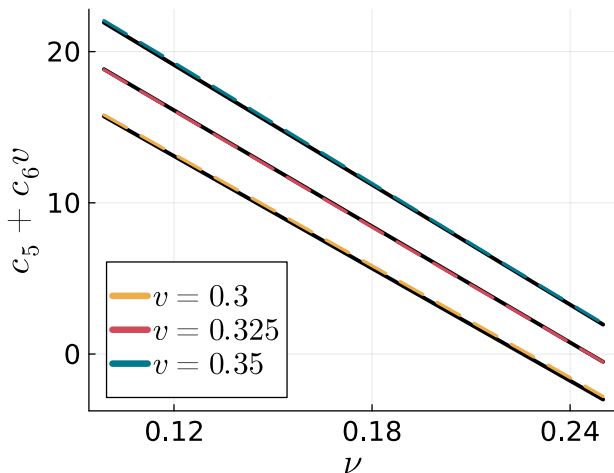


FIG. 5. Comparison of the true and neural-network-learned coefficients for the missing term in the \dot{v} expansion. Solid lines represent the true value while dashed lines the learned coefficients. Different colors corresponding to different values of v . The close agreement between the true and learned curves across different values of v demonstrates that the network successfully recovers the missing higher-order orbital corrections despite the degeneracy between orbital and waveform mode corrections.

³ In the machine learning context, *epochs* and *iterations* are distinct: an epoch corresponds to a forward pass through all training samples, whereas an iteration refers to a single parameter update after processing a batch of data. Since our training does not use mini-batching, the two terms are equivalent in this work.

This experiment establishes a baseline for the framework, demonstrating that the neural network can successfully reproduce analytically known higher order PN terms before being extended to the full PN \rightarrow NR case described in Sec. III.

III. PN \rightarrow NR

A. Overview

Building upon the 2PN \rightarrow 3PN experiment, we extend the framework to bridge the gap between PN approximations and NR waveforms. For the PN baseline, we adopt the TaylorT4 approximant [56] truncated at 4.5PN order [57, 58] as implemented in the `PostNewtonian.jl` package [59].

For the target NR data, we use the `NRHybSur3dq8` [37] surrogate model, which reproduces NR waveforms from the SXS catalog [10] with high fidelity and serves as a computationally efficient proxy for direct NR simulations. To construct the training dataset, we generate a set of nonspinning BBH waveforms using `NRHybSur3dq8`. Specifically, we sample ten systems uniformly in symmetric mass ratio $\nu \in [0.109, 0.25]$, corresponding to mass ratio $q \in [1, 8]$. Each waveform is initialized at a reference (2, 2) mode frequency of $f_{2,2} = 0.00497[1/M]$, which approximately corresponds to an orbital velocity $v \simeq 0.25$ in the PN expansion.

The dataset is then divided into eight training waveforms and two validation waveforms.⁴ These correspond to training mass ratios $q \in \{1.0, 1.7, 2.2, 2.6, 4.5, 5.4, 6.5, 8.0\}$ and validation mass ratios $q \in \{3.2, 3.8\}$. The training waveforms are used to compute the loss that drives optimization, while the validation waveforms provide an independent validation loss that is used solely for monitoring generalization during training. For the final assessment of model performance, we additionally generate a set of 100 waveforms uniformly sampled in $q \in [1, 8]$ and evaluate the trained model on these waveforms. This larger resampled set provides a more robust estimate of the final modeling error and of the model’s generalization quality across the mass ratio range.

Although the overall framework remains largely unchanged from the 2PN \rightarrow 3PN problem, one vital addition is a small neural network branch that outputs ν -dependent corrections to the total mass of the system, M . The motivation for introducing this term is that the definition of black hole masses does not translate directly between PN and NR. In NR simulations, the black hole mass can be defined as the Christodoulou mass computed from the

⁴ This small set of validation waveforms is a holdover from previous experiments and is not optimized for this problem. Future work could explore more robust validation strategies.

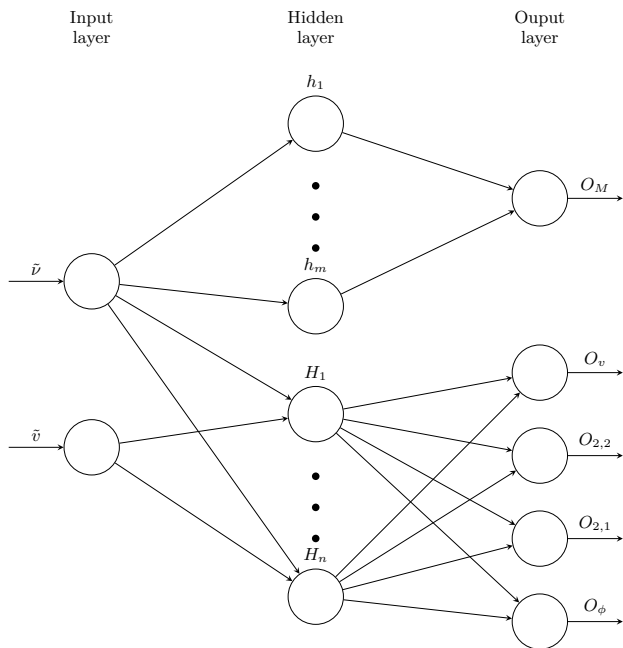


FIG. 6. Neural network architecture for the PN→NR experiment. The two inputs (ν, v) are linearly scaled to the interval $[-1, 1]$ to improve numerical stability during training. Each output is further rescaled by a tunable scaling coefficient before being applied as a correction to the orbital dynamics or waveform modes. The final model uses 4 neurons in the mass-correction branch and 12 neurons in the orbital/mode-correction branch, totaling 101 trainable parameters.

apparent horizons at a reference time, whereas in the PN approximation each black hole is treated as a point particle. To account for discrepancies arising from inconsistent mass definitions, we introduce a learned correction to the total mass. The complete architecture of the extended neural network, including this additional mass correction branch, is shown in Fig. 6.

The overall PN→NR procedure can be summarized as follows:

1. Apply the total mass correction O_M to M_1, M_2 :

$$\begin{aligned} M_1 &= \frac{q}{1+q} (1.0 + \beta_M O_M(\nu)) \\ M_2 &= \frac{1}{1+q} (1.0 + \beta_M O_M(\nu)) \end{aligned} \quad (7)$$

2. Apply the orbital correction $O_v(\nu, v)$ to the 4.5PN expression for \dot{v}
3. Integrate the ODE with the corrected \dot{v} to obtain the corrected orbital evolution.
4. Compute the waveform modes $h_{2,2}$ and $h_{2,1}$ from the corrected orbital solution.
5. Apply the waveform mode corrections as described in Eq. (3)

As in the previous experiment, the inputs are linearly scaled to the interval $[-1, 1]$ to ensure well-conditioned gradients during training. Each neural network output is further multiplied by a tunable scaling coefficient β before being applied as corrections to M, \dot{v} , or the waveform modes $h_{2,2}$ and $h_{2,1}$. The specific values adopted in the final model are summarized in Table I. Several

TABLE I. Hyperparameters used in the final neural network model.

| Hyperparameter | Value |
|----------------|-----------|
| β_M | 10^{-3} |
| β_v | 10^2 |
| $\beta_{2,2}$ | 10^{-2} |
| $\beta_{2,1}$ | 10^{-2} |
| β_ϕ | 10^{-3} |

modifications to the loss function are also introduced and are discussed in detail in Sec. III B.

For the training, we initially tested a two-staged strategy where we first trained on segmented waveform data and then fine-tuning with full waveform data, similar to the 2PN→3PN problem in Sec. II. However, this method proved ineffective for the present problem.⁵ Instead, introducing a new v dependent loss term yields more robust and efficient training, as we will discuss in more details in Sec III B.

As mentioned earlier, we estimate the modeling error by evaluating the network on a set of 100 surrogate-generated waveforms uniformly sampled in mass ratio $q \in [1, 8]$. The evolution of these waveform mismatches over training epochs is shown in Fig. 7. The model quickly reproduces fiducial surrogate waveforms with a mean mismatch of order 10^{-5} after roughly 2000 epochs. Beyond this point, however, the training and validation losses begin to diverge, and the generalization quality degrades. This discrepancy reaches a clear peak at epoch 4000, as shown in Fig. 8, before beginning to decrease again with a rapid drop in the validation loss. By epoch 8000, the training and validation losses have converged, and the resulting mismatches settle to a uniform spread at the 10^{-6} level across the resampled waveforms.

The 4000-epoch point coincides with a checkpoint at which we restart the optimization. The warm restart retains the optimized parameters but resets the inverse Hessian approximation and gradient information. To verify that the turnover at 4000 epoch is not an artifact of restarting, we additionally performed a continuous 8000-epoch run with no restarts. This run exhibits the same peak and subsequent decline at 4000 epochs, confirming that the feature is intrinsic to the optimization landscape, rather than the restart. Notably, the checkpoint warm

⁵ Unlike the smooth and analytically defined 2PN→3PN correction, the PN→NR discrepancy is highly nonlinear and cumulative. Segment-wise training thus overemphasizes local residuals and produces inconsistent corrections across segments.

restart run shows better agreement between the training and validation losses by epoch 8000, suggesting that the restart helps stabilize the late-stage optimization.

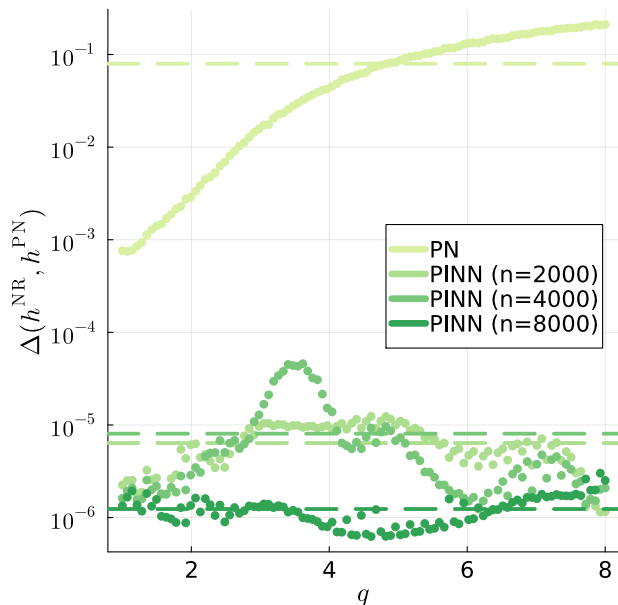


FIG. 7. Evolution of the waveform mismatch during training for the PN \rightarrow NR model. Dashed lines indicate the average mismatch over all mass ratios q . The mismatch decreased rapidly during the early phase of training and eventually converges to a similar level across all values of mass ratio, q . This suggests that the network learns a consistent correction rather than overfitting to a specific mass ratios.

B. Loss Function

The definition of the loss function plays a central role in ensuring that the learned corrections remain physically meaningful and numerically stable across the entire training domain. Beyond the standard mean-squared error between the target and predicted waveforms, a couple additional physics-informed and regularization components are incorporated.

We first describe how the waveform mismatches are actually calculated and incorporated into the overall loss. The waveform mismatch component of the total loss is defined as:

$$\langle \mathcal{L}_w \rangle = \left\langle \frac{\|h_{2,2}^{\text{NR}} - h_{2,2}^{\text{PINN}}\|^2 + \|h_{2,1}^{\text{NR}} - h_{2,1}^{\text{PINN}}\|^2}{\|h_{2,2}^{\text{NR}}\|^2 + \|h_{2,1}^{\text{NR}}\|^2} \right\rangle, \quad (8)$$

where $\langle \rangle$ denotes the average over all training samples and $\| \cdot \|$ follows Eq. (5). Note that this form of waveform mismatch where the contributions from (2, 2) and (2, 1) modes are summed represents averaging waveform mismatch across all points on a sphere.

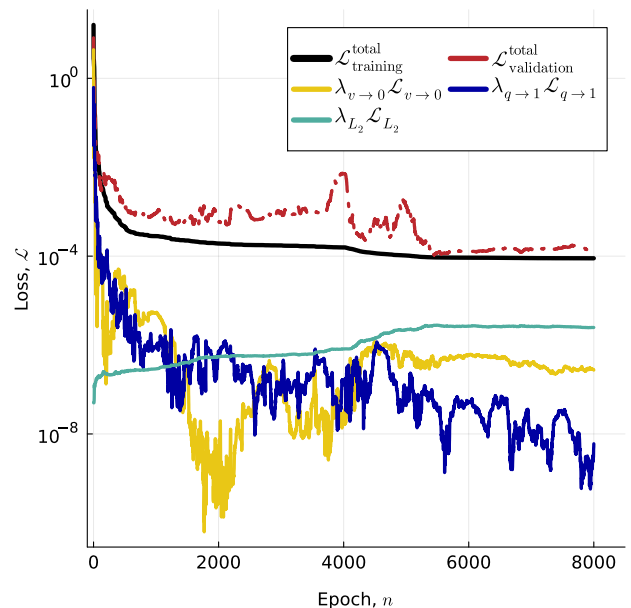


FIG. 8. The history of the total loss and its main components. The losses decrease rapidly during the first 2000 epochs, after which a divergence between training and validation becomes apparent and peaks near 4000 epochs. A warm restart at this point resets the Hessian approximation, restores alignment between the two losses, and leads to improved generalization in the subsequent optimization.

We next impose physically motivated regularization terms that enforce the corrections to vanish in the appropriate limits. Specifically, the orbital and waveform corrections $O_v, O_{2,2}, O_{2,1}, O_\phi \rightarrow 0$ as $v \rightarrow 0$ are required to approach zero as $v \rightarrow 0$ and the subdominant (2, 1) mode correction $O_{2,1}$ must also vanish as the system approaches equal masses ($q \rightarrow 1$). To encode these behaviors, we introduce two additional loss terms, $\mathcal{L}_{v \rightarrow 0}$ and $\mathcal{L}_{q \rightarrow 1}$, defined below.

The first term, $\mathcal{L}_{v \rightarrow 0}$ penalizes nonzero network outputs at $v = 0$ across ten uniformly spaced mass ratios $q \in [1, 8]$:

$$\mathcal{L}_{v \rightarrow 0} = \sum_{\nu(q=8)}^{\nu(q=1)} \left(|O_v(\nu, 0)|^2 + |O_{2,2}(\nu, 0)|^2 + |O_{2,1}(\nu, 0)|^2 + |O_\phi(\nu, 0)|^2 \right) \quad (9)$$

The second term, $\mathcal{L}_{q \rightarrow 1}$ enforces that the (2, 1) mode correction smoothly vanishes in the equal-mass limit. For this term, we evaluate $O_{2,1}$ at ten uniformly spaced $v \in [0.24, 0.38]$ and penalize any nonzero outputs:

$$\mathcal{L}_{q \rightarrow 1} = \sum_{v=0.24}^{0.38} |O_{2,1}(0.25, v)|^2 \quad (10)$$

To further encourage physical consistency between the

PN and NR orbital dynamics, we introduce an auxiliary term that compares the orbital velocity of PN evolution with that inferred from the (2, 2) mode frequency of the NR waveform. This term promotes better phase alignment between the PN and NR waveforms.

We define the NR orbital velocity as

$$v_{\text{NR}} = \omega_{\text{orb}}^{1/3} = (\pi f_{2,2})^{1/3}. \quad (11)$$

This is a combination of two approximations: 1. Kepler's Law and 2. that the orbital and (2, 2)-mode frequency can be trivially related. With this, the orbital velocity loss term is

$$\langle \mathcal{L}_v \rangle = \left\langle \frac{\|v_{\text{NR}} - v_{\text{PN}}\|^2}{\|v_{\text{NR}}\|^2} \right\rangle \quad (12)$$

where $\langle \rangle$ again denotes the average over all training samples and $\| \cdot \|$ follows Eq. (5).

Lastly, we add L_2 regularization terms, proportional to the squared L_2 norms of neural network weights (we exclude the biases). This term mitigates overfitting and improves generalization. We can fine-tune the strength of this regularization term with the hyperparameter λ_{L_2} .

Combining all terms, the total loss function is

$$\begin{aligned} \mathcal{L} = & \lambda_w \langle \mathcal{L}_w \rangle + \lambda_v \langle \mathcal{L}_v \rangle + \lambda_{q \rightarrow 1} \mathcal{L}_{q \rightarrow 1} \\ & + \lambda_{v \rightarrow 0} \mathcal{L}_{v \rightarrow 0} + \lambda_{L_2} \sum_n |\theta_n^{\text{NN}}|^2. \end{aligned} \quad (13)$$

The inclusion of these physically motivated components plays a crucial role in constraining the behavior of learned corrections. The vanishing-limit penalty for $v \rightarrow 0$ ensures that the network respects known agreement between PN and NR in the early inspiral and prevents unphysical extrapolations at small v that are not represented in the training data. Similarly, enforcing the equal-mass limit for the (2, 1)-mode amplitude corrections ensures smooth and consistent behavior as $q \rightarrow 1$, compensating for the fact that the physical (2, 1) mode itself vanishes in this limit and thus lacks a natural boundary condition.

In the final model, we adopt the loss hyperparameter values listed in Table II. These coefficients control the relative weighting of the loss components and were selected through empirical experimentation to achieve a balance between physical fidelity, numerical stability, and optimization efficiency. The relative magnitudes were tuned to ensure that the loss terms and their gradients are of comparable scale at the start of training. Small adjustments to these parameters can noticeably affect the convergence behavior, reflecting the commonly observed sensitivity of neural-network optimization to hyperparameter choices.

C. Extrapolation

In addition to modeling well within the training region, the model exhibits encouraging signs of extrapolation

TABLE II. Loss-function hyperparameters used in the final model.

| Hyperparameter | Value |
|-----------------------------|-----------|
| λ_w | 10^2 |
| λ_v | 10^3 |
| $\lambda_{v \rightarrow 0}$ | 1 |
| $\lambda_{q \rightarrow 1}$ | 1 |
| λ_{L_2} | 10^{-9} |

capabilities. As shown in Fig. 9, the trained NN corrections significantly reduce the mismatch between PN and NR waveforms at higher mass ratios ($q \geq 8$), improving from the 10^{-1} level to roughly 10^{-4} – 10^{-3} . Even though the NN was trained only on the same range ($q \in [1, 8]$) as NRHybSur3dq8, it performs noticeably better in this higher q regime.

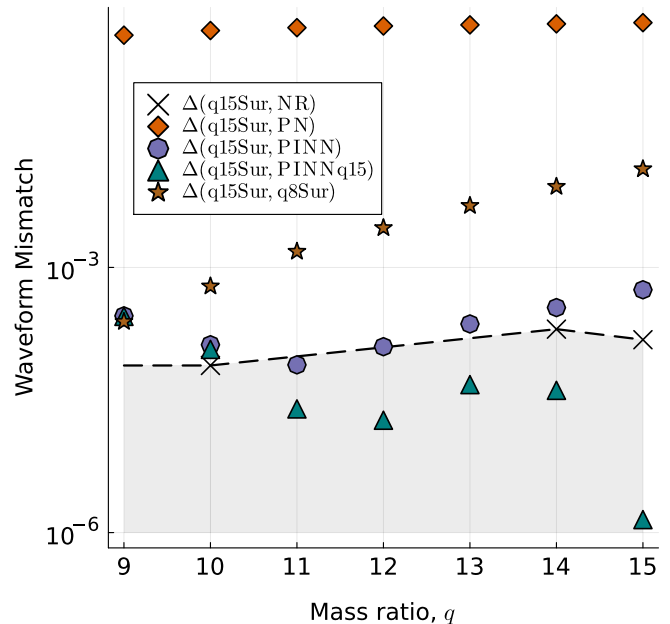


FIG. 9. Waveform mismatches for mass ratios $q \geq 8$ computed against the NRHybSur2dq15, surrogate. Results are shown for the PN baseline, PINN model trained on $q \in [1, 8]$, its extended version with an additional training point at $q = 15$, and the NRHybSur3dq8 surrogate. Although both the original PINN and NRHybSur3dq8 were trained over the same range, the PINN model exhibits better agreement with NRHybSur2dq15 at high mass ratios. Incorporating a single additional $q = 15$ training point further improves waveform accuracy across the intermediate region ($9 \lesssim q \lesssim 15$), reducing mismatches toward the reference level. The dashed lines denotes the mismatch level between NR and NRHybSur2dq15, which serves as the effective reference limit for extrapolation accuracy.

We use the NRHybSur2dq15 surrogate [60], which is trained on hybrid PN-NR waveforms up to mass ratio $q = 15$, as a proxy for NR to assess extrapolation performance. For reference, we also include the mismatch between NR simulations and NRHybSur2d15. Since the NRHybSur2d15

serves here as the effective “ground truth”, it would not be meaningful for our PINN model to achieve errors below this reference. The shaded region therefore marks the range below which further improvement has no physical significance. While our results extend slightly outside of this region, their close proximity demonstrates that the framework generalizes reasonably well beyond its training region.

D. Extending the Model

Building on the model’s demonstrated extrapolation capability, we next investigate how incorporating an additional training data affects its performance. In the original setup, the network was trained on eight systems with mass ratios $q \in [1, 8]$. We now introduce a single additional training waveform at $q = 15$, well separated from the original training range, and examine how the model’s accuracy changes across intermediate mass ratios.

To isolate the impact of this new data point, we keep the original training dataset unchanged and simply append the $q = 15$ waveform generated using NRHybSur2dq15. Starting from the previously trained network parameters, we resume optimization for an additional 4000 epochs using the same loss function and hyperparameters. This warm start allows the network to incorporate new high- q constraints while preserving the structure learned over $q \in [1, 8]$. Throughout this extended training, we verify that the model’s performance within the original training region remains stable.

As shown by the green triangles in Fig. 9, incorporating a single additional training waveform greatly improves the model’s agreement with NRHybSur2dq15 for $q \in [9, 14]$. This result demonstrates the framework’s potential to be efficiently extended by incorporating only a small number of sparsely sampled training data, enabling systematic improvement of model accuracy without requiring dense coverage of the parameter space.

IV. CONCLUSION

We developed a physics-informed neural network by adding a neural network to the post-Newtonian (PN) orbital evolution equations and waveform computations to reduce the difference between PN and numerical relativity (NR). Using the 4.5PN TaylorT4 PN waveforms as the

baseline PN model and restricting to nonspinning systems, we are able to reduce the mismatch between PN and NR from 0.1 to 1×10^{-6} . Our loss function not only includes the waveform mismatch, but also several terms that weakly enforce physical constraints to aid in extrapolation, as well as an L_2 regularization term of the NN weights.

A notable aspect of this study is that the model achieves these results while being trained on only eight waveforms. This demonstrates the data efficiency made possible by embedding physical structure directly into the model, and suggests that such framework may enable the direct use of NR simulations for training even when only a sparse set of waveforms is available. Since the model we present here is physics-informed, i.e., it solves PN equations with (small) corrections, one would expect improved extrapolation compared to a more data-driven model like surrogates. We find that the network maintains lower mismatch than the surrogate model (NRHybSur3dq8) outside of the training region, achieving $10^{-4} - 10^{-3}$ mismatch levels. Moreover, adding a single additional training point at $q = 15$ substantially improves performance across intermediate map ratios, demonstrating that the framework can be efficiently extended with only sparsely sampled data.

Our results demonstrate that physics-informed neural networks provide a promising avenue for bridging the gap between PN theory and NR. Future work will focus on extending the current framework to include spin and eccentricity, as well as extending the framework through merger and ringdown.

ACKNOWLEDGMENTS

This material is based upon work supported by the National Science Foundation under Grants No. PHY-2407742, No. PHY-2207342, and No. OAC-2209655. Any opinions, findings, and conclusions or recommendations expressed in this material are those of the author(s) and do not necessarily reflect the views of the National Science Foundation. This work was supported by the Sherman Fairchild Foundation. This project made use of `Julia` packages including `PostNewtonian.jl` [59], `Lux.jl` [61], `Optimization.jl` [62], `ForwardDiff.jl` [63], `DifferentialEquations.jl` [64], and `Plots.jl` [65]. This project made use of `Python` packages including `gwsurrogate` [66], `NumPy` [67], and `SciPy` [68].

[1] B. P. Abbott *et al.* (LIGO Scientific, Virgo), *Phys. Rev. Lett.* **116**, 061102 (2016), arXiv:1602.03837 [gr-qc].
 [2] arXiv:2509.08099 [gr-qc].
 [3] P. Amaro-Seoane *et al.* (LISA), arXiv:1702.00786 [astro-ph.IM].
 [4] D. Reitze *et al.*, *Bull. Am. Astron. Soc.* **51**, 035 (2019), arXiv:1907.04833 [astro-ph.IM].

[5] M. Punturo *et al.*, *Proceedings, 14th Workshop on Gravitational wave data analysis (GWDAW-14): Rome, Italy, January 26-29, 2010*, *Class. Quant. Grav.* **27**, 194002 (2010).
 [6] F. Pretorius, *Phys. Rev. Lett.* **95**, 121101 (2005), arXiv:gr-qc/0507014 [gr-qc].
 [7] M. Campanelli, C. O. Lousto, P. Marronetti, and Y. Zlo-

- chower, *Phys. Rev. Lett.* **96**, 111101 (2006), arXiv:gr-qc/0511048 [gr-qc].
- [8] J. G. Baker, J. Centrella, D.-I. Choi, M. Koppitz, and J. van Meter, *Phys. Rev. Lett.* **96**, 111102 (2006), arXiv:gr-qc/0511103 [gr-qc].
- [9] SXS Collaboration, The SXS collaboration catalog of gravitational waveforms, <http://www.black-holes.org/waveforms>.
- [10] M. A. Scheel *et al.*, *Class. Quant. Grav.* **42**, 195017 (2025), arXiv:2505.13378 [gr-qc].
- [11] A. Buonanno and T. Damour, *Phys. Rev.* **D59**, 084006 (1999), arXiv:gr-qc/9811091 [gr-qc].
- [12] A. Buonanno and T. Damour, *Phys. Rev.* **D62**, 064015 (2000), arXiv:gr-qc/0001013 [gr-qc].
- [13] A. Buonanno, Y. Chen, and T. Damour, *Phys. Rev. D* **74**, 104005 (2006), arXiv:gr-qc/0508067.
- [14] T. Damour, P. Jaranowski, and G. Schafer, *Phys. Rev. D* **62**, 084011 (2000), arXiv:gr-qc/0005034.
- [15] T. Damour, *Phys. Rev. D* **64**, 124013 (2001), arXiv:gr-qc/0103018.
- [16] A. Buonanno and B. S. Sathyaprakash, Sources of Gravitational Waves: Theory and Observations (2014) arXiv:1410.7832 [gr-qc].
- [17] T. Damour, *Int. J. Mod. Phys. A* **23**, 1130 (2008), arXiv:0802.4047 [gr-qc].
- [18] A. Ramos-Buades, A. Buonanno, H. Estellés, M. Khalil, D. P. Mihaylov, S. Ossokine, L. Pompili, and M. Shiferaw, *Phys. Rev. D* **108**, 124037 (2023), arXiv:2303.18046 [gr-qc].
- [19] S. Khan, S. Husa, M. Hannam, F. Ohme, M. Pürrer, X. Jiménez Forteza, and A. Bohé, *Phys. Rev.* **D93**, 044007 (2016), arXiv:1508.07253 [gr-qc].
- [20] S. Husa, S. Khan, M. Hannam, M. Pürrer, F. Ohme, X. Jiménez Forteza, and A. Bohé, *Phys. Rev.* **D93**, 044006 (2016), arXiv:1508.07250 [gr-qc].
- [21] M. Hannam, P. Schmidt, A. Bohé, L. Haegel, S. Husa, F. Ohme, G. Pratten, and M. Pürrer, *Phys. Rev. Lett.* **113**, 151101 (2014), arXiv:1308.3271 [gr-qc].
- [22] G. Pratten *et al.*, *Phys. Rev. D* **103**, 104056 (2021), arXiv:2004.06503 [gr-qc].
- [23] G. Pratten, S. Husa, C. Garcia-Quiros, M. Colleoni, A. Ramos-Buades, H. Estelles, and R. Jaume, *Phys. Rev. D* **102**, 064001 (2020), arXiv:2001.11412 [gr-qc].
- [24] P. Ajith *et al.*, *Gravitational wave data analysis. Proceedings: 11th Workshop, GWDAW-11, Potsdam, Germany, Dec 18-21, 2006*, *Class. Quant. Grav.* **24**, S689 (2007), arXiv:0704.3764 [gr-qc].
- [25] P. Ajith *et al.*, *Phys. Rev. D* **77**, 104017 (2008), [Erratum: *Phys. Rev. D* **79**, 129901 (2009)], arXiv:0710.2335 [gr-qc].
- [26] P. Ajith *et al.*, *Phys. Rev. Lett.* **106**, 241101 (2011), arXiv:0909.2867 [gr-qc].
- [27] L. Santamaria *et al.*, *Phys. Rev.* **D82**, 064016 (2010), arXiv:1005.3306 [gr-qc].
- [28] L. London, S. Khan, E. Fauchon-Jones, C. García, M. Hannam, S. Husa, X. Jiménez-Forteza, C. Kalaghatgi, F. Ohme, and F. Pannarale, *Phys. Rev. Lett.* **120**, 161102 (2018), arXiv:1708.00404 [gr-qc].
- [29] S. Khan, K. Chatziioannou, M. Hannam, and F. Ohme, *Phys. Rev. D* **100**, 024059 (2019), arXiv:1809.10113 [gr-qc].
- [30] S. Khan, F. Ohme, K. Chatziioannou, and M. Hannam, *Phys. Rev. D* **101**, 024056 (2020), arXiv:1911.06050 [gr-qc].
- [31] T. Dietrich, S. Khan, R. Dudi, S. J. Kapadia, P. Kumar, A. Nagar, F. Ohme, F. Pannarale, A. Samajdar, S. Bernuzzi, G. Carullo, W. Del Pozzo, M. Haney, C. Markakis, M. Pürrer, G. Riemenschneider, Y. E. Setyawati, K. W. Tsang, and C. Van Den Broeck, *Phys. Rev. D* **99**, 024029 (2019), arXiv:1804.02235 [gr-qc].
- [32] T. Dietrich, A. Samajdar, S. Khan, N. K. Johnson-McDaniel, R. Dudi, and W. Tichy, *Phys. Rev. D* **100**, 044003 (2019), arXiv:1905.06011 [gr-qc].
- [33] J. E. Thompson, E. Fauchon-Jones, S. Khan, E. Nitoglia, F. Pannarale, T. Dietrich, and M. Hannam, *Phys. Rev. D* **101**, 124059 (2020), arXiv:2002.08383 [gr-qc].
- [34] C. García-Quirós, M. Colleoni, S. Husa, H. Estellés, G. Pratten, A. Ramos-Buades, M. Mateu-Lucena, and R. Jaume, *Phys. Rev. D* **102**, 064002 (2020), arXiv:2001.10914 [gr-qc].
- [35] C. García-Quirós, S. Husa, M. Mateu-Lucena, and A. Borchers, *Class. Quant. Grav.* **38**, 015006 (2021), arXiv:2001.10897 [gr-qc].
- [36] J. Blackman, S. E. Field, C. R. Galley, B. Szilágyi, M. A. Scheel, M. Tiglio, and D. A. Hemberger, *Phys. Rev. Lett.* **115**, 121102 (2015), arXiv:1502.07758 [gr-qc].
- [37] V. Varma, S. E. Field, M. A. Scheel, J. Blackman, L. E. Kidder, and H. P. Pfeiffer, *Phys. Rev.* **D99**, 064045 (2019), arXiv:1812.07865 [gr-qc].
- [38] J. Blackman, S. E. Field, M. A. Scheel, C. R. Galley, D. A. Hemberger, P. Schmidt, and R. Smith, *Phys. Rev.* **D95**, 104023 (2017), arXiv:1701.00550 [gr-qc].
- [39] J. Blackman, S. E. Field, M. A. Scheel, C. R. Galley, C. D. Ott, M. Boyle, L. E. Kidder, H. P. Pfeiffer, and B. Szilágyi, *Phys. Rev.* **D96**, 024058 (2017), arXiv:1705.07089 [gr-qc].
- [40] V. Varma, S. E. Field, M. A. Scheel, J. Blackman, D. Gerosa, L. C. Stein, L. E. Kidder, and H. P. Pfeiffer, *Phys. Rev. Research.* **1**, 033015 (2019), arXiv:1905.09300 [gr-qc].
- [41] D. Sun, M. Boyle, K. Mitman, M. A. Scheel, L. C. Stein, S. A. Teukolsky, and V. Varma, *Phys. Rev. D* **110**, 104076 (2024), arXiv:2403.10278 [gr-qc].
- [42] D. Sun and L. C. Stein, Parameter matching between horizon quasi-local and point-particle definitions at 1PN for quasi-circular and non spinning BBH systems in harmonic gauge (2025), arXiv:2510.25618 [gr-qc].
- [43] L. M. Thomas, K. Chatziioannou, V. Varma, and S. E. Field, *Phys. Rev. D* **111**, 104029 (2025), arXiv:2501.16462 [gr-qc].
- [44] L. Negri and A. Samajdar, arXiv:2509.17606 [astro-ph.HE].
- [45] R. Singh and S. Sharma, 2025 3rd International Conference on Sustainable Computing and Data Communication Systems (ICSCDS) , 1547 (2025).
- [46] A. Ghosh, H. Behl, E. Dupont, P. Torr, and V. Namboodiri, in *Advances in Neural Information Processing Systems*, Vol. 33, edited by H. Larochelle, M. Ranzato, R. Hadsell, M. F. Balcan, and H. Lin (Curran Associates, Inc., 2020) p. 14831–14843.
- [47] C. Coelho, M. F. P. Costa, and L. L. Ferrás, *Expert Systems with Applications* **273**, 126784 (2025).
- [48] P. Marion, Generalization bounds for neural ordinary differential equations and deep residual networks (2023), arXiv:2305.06648 [stat.ML].
- [49] C. Rackauckas, Y. Ma, J. Martensen, C. Warner, K. Zubov, R. Supekar, D. Skinner, A. Ramadhan, and A. Edelman, Universal differential equations for scientific machine learning (2021), arXiv:2001.04385 [cs.LG].
- [50] J. Bolibar, F. Sapienza, F. Maussion, R. Lguensat,

- B. Wouters, and F. Pérez, *Geoscientific Model Development* **16**, 6671–6687 (2023).
- [51] M. Zhu, H. Zhang, A. Jiao, G. E. Karniadakis, and L. Lu, *Computer Methods in Applied Mechanics and Engineering* **412**, 10.1016/j.cma.2023.116064 (2023).
- [52] E. C. Rodrigues, R. L. Thompson, D. A. B. Oliveira, and R. F. Ausas, *Finding the underlying viscoelastic constitutive equation via universal differential equations and differentiable physics* (2025), arXiv:2501.00556 [physics.flu-dyn].
- [53] T. Kapoor, A. Chandra, D. M. Tartakovsky, H. Wang, A. Nunez, and R. Dollevoet, *Neural oscillators for generalization of physics-informed machine learning* (2023), arXiv:2308.08989 [cs.LG].
- [54] B. Keith, A. Khadse, and S. E. Field, *Phys. Rev. Res.* **3**, 043101 (2021), arXiv:2102.12695 [gr-qc].
- [55] D. P. Kingma, arXiv preprint arXiv:1412.6980 (2014).
- [56] M. Boyle, D. A. Brown, L. E. Kidder, A. H. Mroue, H. P. Pfeiffer, M. A. Scheel, G. B. Cook, and S. A. Teukolsky, *Phys. Rev.* **D76**, 124038 (2007), arXiv:0710.0158 [gr-qc].
- [57] L. Blanchet, G. Faye, Q. Henry, F. Larrouturou, and D. Trestini, *Phys. Rev. Lett.* **131**, 121402 (2023), arXiv:2304.11185 [gr-qc].
- [58] L. Blanchet, G. Faye, Q. Henry, F. Larrouturou, and D. Trestini, *Phys. Rev. D* **108**, 064041 (2023), arXiv:2304.11186 [gr-qc].
- [59] M. Boyle, *PostNewtonian.jl* (2024).
- [60] J. Yoo, V. Varma, M. Giesler, M. A. Scheel, C.-J. Haster, H. P. Pfeiffer, L. E. Kidder, and M. Boyle, *Phys. Rev. D* **106**, 044001 (2022), arXiv:2203.10109 [gr-qc].
- [61] A. Pal, *Lux: Explicit Parameterization of Deep Neural Networks in Julia* (2023), if you use this software, please cite it as below.
- [62] V. K. Dixit and C. Rackauckas, *Optimization.jl: A unified optimization package* (2023).
- [63] J. Revels, M. Lubin, and T. Papamarkou, arXiv:1607.07892 [cs.MS] (2016).
- [64] C. Rackauckas and Q. Nie, *Journal of Open Research Software* **5** (2017).
- [65] S. Christ, D. Schwabeneder, C. Rackauckas, M. Borregaard, and T. Breloff, *Journal of Open Research Software* **11**, 5 (2023), arXiv:2204.08775.
- [66] S. E. Field *et al.*, *J. Open Source Softw.* **10**, 7073 (2025), arXiv:2504.08839 [astro-ph.IM].
- [67] C. R. Harris, K. J. Millman, S. J. van der Walt, R. Gommers, P. Virtanen, D. Cournapeau, E. Wieser, J. Taylor, S. Berg, N. J. Smith, R. Kern, M. Picus, S. Hoyer, M. H. van Kerkwijk, M. Brett, A. Haldane, J. F. del Río, M. Wiebe, P. Peterson, P. Gérard-Marchant, K. Sheppard, T. Reddy, W. Weckesser, H. Abbasi, C. Gohlke, and T. E. Oliphant, *Nature* **585**, 357 (2020).
- [68] P. Virtanen, R. Gommers, T. E. Oliphant, M. Haberland, T. Reddy, D. Cournapeau, E. Burovski, P. Peterson, W. Weckesser, J. Bright, S. J. van der Walt, M. Brett, J. Wilson, K. J. Millman, N. Mayorov, A. R. J. Nelson, E. Jones, R. Kern, E. Larson, C. J. Carey, Í. Polat, Y. Feng, E. W. Moore, J. VanderPlas, D. Laxalde, J. Perktold, R. Cimrman, I. Henriksen, E. A. Quintero, C. R. Harris, A. M. Archibald, A. H. Ribeiro, F. Pedregosa, P. van Mulbregt, and SciPy 1.0 Contributors, *Nature Methods* **17**, 261 (2020).